

Banner appropriate to article type will appear here in typeset article

1 A mathematical model for limit-cycle 2 switching in open cavity flow

3 Prabal S. Negi[†]

**4 Okinawa Institute of Science and Technology Graduate University, Onna, Okinawa 904-0495,
5 Japan**

6 (Received xx; revised xx; accepted xx)

**7 A reduced mathematical model for the flow in an open cavity is presented.
8 The reduction is based on the center manifold theory applied to a perturbation
9 of the original system. The model exhibits many of the key characteristics
10 observed in the flow dynamics including unstable quasi-periodic edge states
11 as well as switching of stability of the limit cycles. The model explains the
12 mechanism behind the switching of stability of the limit cycles and also predicts
13 the bifurcation points where such stability switching occurs.**

14 1. Introduction

**15 The two-dimensional shear driven flow over a cavity presents an interesting case
16 of successive bifurcations appearing in a hydrodynamic flow. The flow case has
17 been brought to the attention of the hydrodynamic stability community by Sipp
18 and Lebedev (2007), where, the authors used the geometry to investigate the the-
19 oretical aspects of stability analysis around time averaged mean flows. The case
20 has featured as an object of investigation in various different contexts of stability
21 and control (Rowley and Williams 2006; Sipp et al. 2010; Barbagallo et al. 2009),
22 model reduction (Loiseau and Brunton 2018), self-consistent modeling (Meliga
23 2017), center-manifold reduction (Negi 2024) etc.**

**24 The basic scenario of the case is this - a boundary layer flow is allowed to
25 develop over flat plate which contains a large depression in the form of a square
26 cavity. Up to a Reynolds number of roughly $Re \approx 4130$ (based on the cavity height
27 and freestream velocity) a steady circulation develops within the cavity and the
28 developing boundary layer flows smoothly over this circulation as it crosses the
29 open cavity. Around this Reynolds number range the first bifurcation occurs
30 and the flow exhibits low amplitude oscillations with a characteristic frequency
31 and spatial wavelength. Subsequently at around $Re \approx 4500$ a second bifurcation
32 seems to occur and a distinctly different oscillation frequency and wavelength
33 becomes dominant in the flow. While classic asymptotic methods are able to
34 capture the characteristics of the first bifurcation (Sipp and Lebedev 2007; Negi
35 2024), modeling the second bifurcation is more complicated. Meliga (2017) has
36 shown that using a second-order self-consistent model (Mantić-Lugo et al. 2015),**

[†] Email address for correspondence: prabal.negi@oist.jp

which takes into account higher harmonics is able to capture the flow frequencies occurring after the second bifurcation. While the self-consistent model incorporates many of the aspects of weakly nonlinear analysis, it invokes an assumption of marginal stability of the equilibrium flow which, while intuitively justified, has a somewhat heuristic nature. In addition, mode shapes, amplitudes and equilibrium frequencies are all coupled and require an iterative procedure for the final solution. An interesting and exhaustive investigation of the flow dynamics within this Reynolds number regime has been performed by Bengana et al. (2019). The authors employed several tools within the dynamical systems framework - linear stability, Floquet analysis, mean flow stability analysis and edge tracking to build a comprehensive picture of the successive bifurcations in the flow as the Reynolds number is varied. Besides the two distinct limit cycles, the authors were also able to identify a quasi-periodic state which has been interpreted as a non-linear superposition of the two distinct limit cycles. This quasi-periodic state is the edge state between the two limit cycles although, the authors speculate that the state might in fact be periodic with a very long period.

Despite the detailed analyses of previous studies, a reduced model representing the essential dynamics of the problem has remained out of reach. In Bengana et al. (2019) the authors propose a normal form representation of the dynamics but do not attempt to derive the representation or specify the coefficients. The current work proposes a reduced representation based on the center manifold theory (Carr 1982; Carr and Muncaster 1983; Wiggins 2003; Guckenheimer and Holmes 1983; Roberts 2014). At the bifurcation point one could evaluate the center subspace of the linearized operator and the center manifold as the (nonlinear) continuation of this tangent subspace. However, this system exhibits only a single oscillatory mode in the center subspace. This is obviously insufficient for the representation of the dynamics where two distinct limit cycles oscillations can emerge. Instead, we consider a perturbed system with a codimension two bifurcation point via the introduction of a “pseudo-parameter”. This is fairly straightforward to construct whenever the relevant direct and adjoint tangent vectors are known. The center manifold can now be obtained for the perturbed system asymptotically, with the asymptotic variables also including the new pseudo-parameter in addition to the modal variables (and inverse Reynolds number). The original system is then approximated by replacing the pseudo-parameter by the appropriate value. The approach can be thought of as an example of “backward theory” developed by Hochs and Roberts (2019); Roberts (2022), wherein, the dynamics of the original system on an invariant manifold are approximated by a nearby system’s invariant manifold. Here though, we do not construct the exact invariant manifold but rather an asymptotic one.

2. Open Cavity Flow

The setup of the two-dimensional open cavity flow follows exactly as has been described in Negi (2024), which follows from that of Sipp and Lebedev (2007). Briefly, the domain consists of a square cavity with sides of length one and an open channel flow is constructed above the cavity.

The open channel has a width of 0.5 above the cavity and a symmetry boundary condition is applied to the upper boundary of the channel. A uniform (streamwise) velocity boundary condition of $u = 1$ is applied to the inlet located at $x = -1.2$. A symmetry boundary condition is applied to the lower wall of the channel from

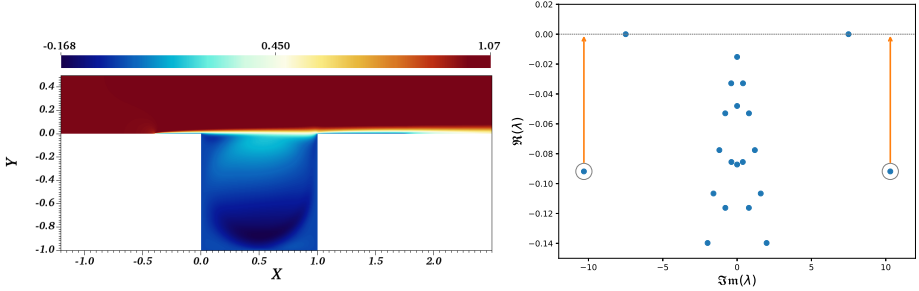


Figure 1: (Left) streamwise velocity of the stationary base flow at $Re_c = 4131.33$ and (right) the spectrum (blue dots) obtained at the bifurcation point.

the inlet to $x = -0.4$ which allows the flow to develop freely from the inlet. A no-slip condition is applied on the lower wall thereafter until $x = 1.75$ (including the cavity walls), after which, a symmetry condition is applied again from $x = 1.75$ to the outlet, located at $x = 2.50$. The continuous system is discretized using the spectral-element-method (Patera 1984) and the Nek5000 code (Fischer et al. 2008) is utilized for the computations.

The critical point for the particular geometry is found to be $Re_c = 4131.33$. There is a slight variability in the literature on the value of the bifurcation point (Sipp and Lebedev 2007; Meliga 2017; Bengana et al. 2019). However all reported are within 1% error of each other, and the calculated value here falls within that range. The base flow at bifurcation is shown in figure 1 (left). The calculated baseflow velocities will be denoted $\mathbf{U}^0 = [\mathbf{U}_x^0; \mathbf{U}_y^0]$ (which includes its two components) and, its associated pressure field is given by, P^0 . Hereafter we will only deal with the deviation from this base flow velocities $\mathbf{u} = [\mathbf{u}_x; \mathbf{u}_y]$ and pressure p , with the total velocity field being $\mathbf{U} = \mathbf{U}^0 + \mathbf{u}$, and the total pressure given by $P = P^0 + p$. The governing equations for the velocity and pressure deviations are given by the Navier–Stokes. Considering the velocity and pressure together as one vector $\bar{\mathbf{u}} = [\mathbf{u}; p]$, we write this compactly as,

$$\begin{aligned} & \partial \bar{\mathbf{u}} / \partial t = \mathbf{L} \bar{\mathbf{u}} + \mathbf{N}(\bar{\mathbf{u}}), \\ & \mathbf{L} = \begin{bmatrix} \operatorname{Re}^{-1} \nabla^2 - (\mathbf{U}^0 \cdot \nabla) - (\nabla \mathbf{U}^0) \cdot & -\nabla \\ \nabla \cdot & 0 \end{bmatrix}, \quad \mathbf{N}(\bar{\mathbf{u}}) = \begin{bmatrix} -\mathbf{u} \cdot \nabla \mathbf{u} \\ 0 \end{bmatrix}, \end{aligned} \quad (2.1)$$

where, \mathbf{L} and \mathbf{N} are respectively the linear and non-linear operators at bifurcation. The calculated spectrum at bifurcation is shown in figure 1 (right), which was calculated using the Krylov–Schur algorithm (Stewart 2002). The spectral problem was also solved for the adjoint operator.

A single pair of complex-conjugate neutral modes can be observed in the figure 1, lying on the x -axis line. This pair of modes (numbered 1 and 2), with the eigenvalue $\lambda_{1,2} = \pm 7.495\iota$, governs the dynamics of the first limit cycle that emerges as the system moves just past the bifurcation point (Negi 2024; Bengana et al. 2019). However, deep in the stable spectrum lies another pair of modes with the eigenvalues $\lambda_{3,4} = -0.092 \pm 10.31\iota$, marked by the gray circles. This mode has been found to be responsible for the second limit cycle oscillation that becomes dominant with further increases in Reynolds numbers (Bengana et al. 2019). One can not directly incorporate this mode into the center manifold evaluation of the system given by equation 2.1. However, if one could perturb the system so that

119 modes 3 and 4 are also neutral simultaneously with modes 1 and 2, then one has
 120 a co-dimension 2 bifurcation point and the resulting center manifold would be
 121 the nonlinear continuation of both these pair of modes. Such a system is easily
 122 built. Denoting the direct and adjoint eigenvectors for the modes as $\bar{\mathbf{v}}_i$ and $\bar{\mathbf{w}}_i$,
 123 respectively, with $i \in 1, 2, 3, 4$, one may build a synthetic system as,

124
$$\partial\bar{\mathbf{u}}/\partial t = \tilde{\mathbf{L}}\bar{\mathbf{u}} + \mathbf{N}(\bar{\mathbf{u}}), \quad \tilde{\mathbf{L}} = \mathbf{L} + \sigma(\bar{\mathbf{v}}_3\bar{\mathbf{w}}_3^\dagger + \bar{\mathbf{v}}_4\bar{\mathbf{w}}_4^\dagger) \quad (2.2)$$

125 where \dagger represents the complex-conjugated transpose and σ is the new pseudo-
 126 parameter that has been introduced. The eigenvectors of the new linearized
 127 system $\tilde{\mathbf{L}}$ are identical to those of \mathbf{L} . All eigenvalues except for $\lambda_{3,4}$ are also
 128 identical. The new affected eigenvalues are $\tilde{\lambda}_{3,4} = \lambda_{3,4} + \sigma$. Clearly, if one sets
 129 $\sigma = -\Re(\lambda_{3,4})$, *i.e.* the real part of $\lambda_{3,4}$, then the eigenvalues of these modes gets
 130 mapped to the x -axis, as indicated by the arrows in figure 1. Therefore we now
 131 have a system with a co-dimension two bifurcation.

132 3. A Reduced Representation

133 One may evaluate not just the standard center manifold emanating from the fixed
 134 point of the new system, but also a parameter dependent (usually asymptotic)
 135 center manifold so that variations of Reynolds number can be obtained on a
 136 reduced representation of the system. Typically, one takes the inverse Reynolds
 137 number variation as a small parameter, $\text{Re}^{-1} = \text{Re}_c^{-1}(1 - \epsilon)$, or some variation
 138 thereof, accounting for scaling (Sipp and Lebedev 2007; Carini et al. 2015; Negi
 139 2024). In this case we would also like to consider the variation with respect to
 140 the newly introduced parameter σ . We would therefore consider a perturbation
 141 of this parameter as $\sigma = \sigma_0 + \sigma'$, where $\sigma_0 = -\Re(\lambda_{3,4})$.

142 Parametric (and asymptotic) center manifold evaluation can be performed
 143 in multiple different ways depending on one's preference and style. One could
 144 consider power series expansions in the amplitudes of the center subspace modes
 145 and then augment the power series with additional polynomial terms to account
 146 for the additional parameter perturbations, here ϵ and σ' , as has been done in
 147 Coullet and Spiegel (1983); Roberts (2014); Carini et al. (2015). Alternately, one
 148 could consider extended systems, and include additional trivial equations for the
 149 parameter evolutions, thereby promoting parameter perturbations to intrinsic
 150 center subspace modes of the extended system, an often used trick for small
 151 dynamical systems, with some applications to larger systems as well (Mercer
 152 and Roberts 1990; Cox and Roberts 1991; Negi 2024; Vizzaccaro et al. 2024).
 153 Recently, asymptotic expansions of spectral submanifolds of extended systems
 154 was performed in Vizzaccaro et al. (2024) in the context of external forcing. The
 155 consequences of system extension have been investigated to significant depth in
 156 the context of center manifolds in Negi (2026). The extended systems approach
 157 was taken here. The methodology is described here only conceptually. One may
 158 find detailed exposition of asymptotic evaluation of invariant manifolds in several
 159 works in the literature, see for example, Coullet and Spiegel (1983); Wiggins
 160 (2003); Roberts (2014); Carini et al. (2015); Jain and Haller (2022); Vizzaccaro
 161 et al. (2024); Negi (2024, 2026).

162 Briefly, the solution of equation (2.2) restricted to the center manifold is
 163 assumed to be, $\bar{\mathbf{u}}(t) = \bar{\mathbf{y}}(\mathbf{z}(t))$, where, \mathbf{z} is the vector of dimensionality equal
 164 to the dimensionality of the center subspace (of the extended system). The

time evolution of \mathbf{z} is assumed to be, $\dot{\mathbf{z}} = \mathcal{G}(\mathbf{z})$, where, \mathcal{G} is the sought after reduced representation of the system dynamics. Both $\bar{\mathbf{y}}$ and \mathcal{G} are expanded as a power series in \mathbf{z} , and their substitution into equation (2.2) results in a series of homological equations, that can be solved order by order. To obtain the reduced representation in its normal form, all entries in the asymptotic expansion of \mathcal{G} are set to zero, except those that are required to remove singularities due to resonance terms in the homological equation.

The normal form of the parametric center manifold obtained for the synthetic system is given below,

$$\begin{aligned} \dot{z}_1 &= + (7.495\iota)z_1 + (0.835 + 0.724\iota)z_1\epsilon \\ &\quad + (0.325 + 0.230\iota)z_1(\epsilon)^2 - (0.004 - 0.001\iota)z_1\epsilon\sigma' \\ &\quad - (1553.8 + 342.5\iota)z_1|z_3|^2 - (573.2 - 340.0\iota)z_1|z_1|^2, \end{aligned} \quad (3.1a)$$

$$\begin{aligned} \dot{z}_3 &= + (1.0\sigma' + 10.31\iota)z_3 + (1.801 + 1.096\iota)z_3\epsilon \\ &\quad + (0.631 + 0.395\iota)z_3(\epsilon)^2 - (0.005 - 0.001\iota)z_3\epsilon\sigma' \\ &\quad - (751.0 + 6.987\iota)z_3|z_3|^2 - (829.4 - 275.2\iota)z_3|z_1|^2. \end{aligned} \quad (3.1b)$$

Here, z_1 refers to the amplitude corresponding to the $\tilde{\lambda}_1$ mode and z_3 refers to the amplitude of the $\tilde{\lambda}_3$ mode. The equations for z_2 and z_4 are the corresponding complex conjugates of equation 3.1. As mentioned earlier, ϵ is the perturbation parameter for the Reynolds number, defined using $\text{Re}^{-1} = \text{Re}_c^{-1}(1 - \epsilon)$. This is the normal form of the synthetic system defined in equation (2.2). However, if we consider $\sigma' = -\sigma_0$, the additional terms that were introduced to generate the synthetic system and one obtains the original system that had a co-dimension one bifurcation point. The first term on the right hand side in equation (3.1b) becomes $(-0.092 + 10.31\iota)z_3$, which is precisely the λ_3 eigenvalue of the original system. Henceforth the value of σ' is held fixed and it is treated simply as another constant coefficient term.

The reduced system can be integrated in time to obtain the system response for different Reynolds numbers. This is plotted in figure 2 for $\text{Re} = 4200$, where one could expect the limit cycle associated with $\lambda_{1,2}$ to emerge, and for $\text{Re} = 4500$, where $\lambda_{3,4}$ modes limit-cycles could possibly emerge. The mode amplitudes z_1, z_3 were given a small random initialization and the evolution is tracked. For $\text{Re} = 4200$, the mode amplitude z_3 has decayed to zero and z_1 dominates the system response. On the other hand, for $\text{Re} = 4500$, the situation is reversed and z_3 dominates the system response and z_1 has decayed to zero. The final system frequencies are then determined by the dominating modes at saturation. The peak value of the mode oscillations is plotted for the entire time history in the right most panel in figure 2. The opposing evolution of the two modes at the two different Reynolds numbers is clearly visible.

To further determine the points where the mode switching takes place, one can obtain the evolution equations for the square amplitudes, $|z_1|^2$ and $|z_3|^2$ from equation (3.1), by multiplying each equation by its conjugate variable, *i.e.*, we multiply equation (3.1a) by z_1^* and equation (3.1b) by z_3^* . Utilizing the conjugate equations allows us to get rid of the imaginary terms and one obtains the equations for the squared amplitudes as,

$$\frac{d|z_1|^2}{dt} = (1.669\epsilon + 0.649\epsilon^2 - 0.007\epsilon\sigma' - 3107.6|z_3|^2 - 1146.4|z_1|^2)|z_1|^2, \quad (3.2a)$$

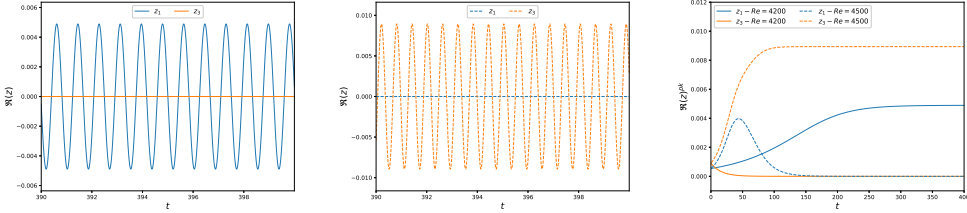


Figure 2: Real part of the time varying response of the reduced system at (left)

Re = 4200 and (center) Re = 4500. The labels z_1 (blue), and z_3 (orange) correspond to the amplitudes of the modes λ_1 and λ_3 respectively. The figure on the right shows the time evolution of peak of the oscillation amplitudes for the two modes z_1, z_3 , and for the two different Reynolds numbers, $Re = 4200$ (solid lines) and $Re = 4500$ (dashed lines).

$$\frac{d|z_3|^2}{dt} = (3.603\epsilon + 2.0\sigma' + 1.262\epsilon^2 - 0.011\epsilon\sigma' - 1502|z_3|^2 - 1658.8|z_1|^2)|z_3|^2. \quad (3.2b)$$

207

These equations can be analyzed for equilibrium when the time derivatives vanish. Since both ϵ and σ' are just treated as constant parameters, equation (3.2) can be analyzed by parametrically plotting the null-clines of the evolution functions on the right hand sides of the two equations, while restricting the analysis to the first-quadrant of the $|z_1| - |z_3|$ phase plane. Obviously, $|z_1| = 0$ and $|z_3| = 0$ are the trivial null-clines for equations (3.2a) and (3.2b) respectively. These represent the complete absence of the respective modes at equilibrium. The non-trivial null-clines, representing limit-cycle oscillation amplitudes are given by,

$$3107.6|z_3|^2 + 1146.4|z_1|^2 = 1.669\epsilon + 0.649\epsilon^2 - 0.007\epsilon\sigma', \quad (3.3a)$$

216

$$1502|z_3|^2 + 1658.8|z_1|^2 = 3.603\epsilon + 2.0\sigma' + 1.262\epsilon^2 - 0.011\epsilon\sigma', \quad (3.3b)$$

that represent a pair of ellipses for the variables $|z_1|$ and $|z_3|$. These non-trivial null-clines will be referred to as the LCO null-clines. At $\epsilon = 0$, representing the bifurcation point, the right hand side (r.h.s) for equation (3.3b) is $2\sigma'$, which is negative, and there are no solutions for this equation. Therefore at bifurcation, no limit-cycle for the $\lambda_{3,4}$ mode exists. The r.h.s for equation (3.3a) is zero, and a trivial solution $z_1 = 0, z_3 = 0$ exists. This of course represents the birth of the first limit-cycle associated with the $\lambda_{1,2}$ mode, as one would expect. Bengana et al. (2019) refer to this as Re_2 . The authors have numbered the important bifurcation events based on the closest limit cycle that can be associated with the event. Here, we follow the numbering sequentially in order of its occurrence as ϵ is increased. To avoid confusion, we will refer to the bifurcation events in this study with an overhead tilde, so the first bifurcation point will be referred to as \widetilde{Re}_1 . As ϵ is increased the r.h.s of equation (3.3a) becomes non-zero and a non-trivial solution of $|z_1|$ can be found, with $|z_3| = 0$ (trivial nullcline), which represents the growing $\lambda_{1,2}$ mode limit-cycle as the system moves away from the bifurcation point.

The next interesting point occurs when $\lambda_{3,4}$ mode limit cycle is born. This occurs when the r.h.s for equation (3.3b) is first non-negative, and $|z_1| = 0$, which occurs for,

$$3.603\epsilon_2 + 2.0\sigma' + 1.262\epsilon_2^2 - 0.011\epsilon_2\sigma' = 0; \implies \epsilon_2 = 0.05; \quad \widetilde{Re}_2 = 4349.6. \quad (3.4)$$

235

236

237

239 Bengana et al. (2019) refer to this as Re_3 and obtain a value of 4348 through a
 240 quadratic approximation, which is remarkably close to the value obtained here.
 241 The null-clines for the system are shown in the first panel from the left in figure 3.
 242 The fixed points are marked using circles, with stable fixed points denoted by
 243 filled circles, while unstable ones denoted by empty circles. Further increases in
 244 Reynolds number result in two distinct LCO null-clines however, these LCO null-
 245 clines intersect only with the trivial null-clines, $|z_1| = 0$ or $|z_3| = 0$. Therefore
 246 no invariant quasi-steady solutions exist so far. The bifurcation to a quasi-steady
 247 solution occurs at $\widetilde{\text{Re}}_3 = 4415.7$, when the two LCO null-clines intersect. This
 248 corresponds to $\text{Re}'_3 = 4410$ in Bengana et al. (2019), which is again close to
 249 the value obtained here. In Bengana et al. (2019) the authors find that around
 250 this bifurcation the characteristics of the quasi-periodic state are much closer to
 251 those of the limit-cycle of the second bifurcation, which they refer to as LC_3
 252 ($\lambda_{3,4}$ -mode LCO in the current study). This is indeed what is found here as well.
 253 The first intersection of the two LCO null-clines occurs for a vanishing value of
 254 z_1 . Therefore, at the inception of the quasi-steady state the $\lambda_{1,2}$ limit cycle has
 255 a vanishingly small amplitude and the quasi-periodic state characteristics will be
 256 dominated by those of the $\lambda_{3,4}$ limit cycle.

257 The quasi-steady solutions have been identified as the edge state between the
 258 two limit cycles in Bengana et al. (2019). As the Reynolds number is further
 259 increased, the edge-state has non-trivial components of both the z_1 and z_3 mode
 260 amplitudes. The edge-state moves along the intersection of the null-clines until
 261 at $\widetilde{\text{Re}}_4 = 4853.8$ the edge state is such that it has a vanishing z_3 component. The
 262 quasi-periodic state ceases to exist beyond this point. In Bengana et al. (2019)
 263 the disappearance of the edge state is found to be at around $\text{Re}'_2 = 4600$,
 264 which is a bit different from what is predicted in the current study. We comment
 265 on this point later in the section. Beyond $\widetilde{\text{Re}}_4$, there exist two distinct fixed points
 266 of the system, one for each limit cycle.

267 The role of the cubic terms in equation (3.1), or the quartic terms in equa-
 268 tion (3.2) is to provide a saturation mechanism for a growing limit-cycle (when
 269 the coefficient of these terms is negative). For a standard Hopf bifurcation, only
 270 a self saturation term exists, $|z_1|^4$ for equation (3.2a) for example, and the
 271 cross interaction term $|z_1|^2|z_3|^2$ is absent. The cross-interaction terms in both
 272 equations (3.2a) and (3.2b) have a negative sign so that the presence of one
 273 mode strengthens the saturation mechanism of the other.

274 Earlier, we identified the second bifurcation in the flow as the first non-trivial
 275 existence of the $\lambda_{3,4}$ LCO, which is the top left panel in figure 3. However, this
 276 bifurcation occurs when $|z_1| = 0$. If we imagine a commonly employed strategy
 277 for analyzing systems, which is to slowly vary a system parameter and observe
 278 the response, the bifurcation scenario looks different. Increasing the Reynolds
 279 number marginally from the first bifurcation point and allowing the system to
 280 equilibrate, means that the system reaches the fixed point lying of the $|z_1|$ axis
 281 in figure 3. The system then follows the fixed point with slow increases of the
 282 Reynolds number. At the second bifurcation point, $\widetilde{\text{Re}}_2$, the $\lambda_{3,4}$ LCO would
 283 emerge (at least transiently) for a quiescent flow state, however, the non zero $|z_1|$
 284 leads to added damping effects and the LCO remains stable. In this scenario, the
 285 $\lambda_{3,4}$ LCO can only emerge when the *effective* eigenvalue for the z_3 evolution starts
 286 having a non-negative real part. This cross-over point can be found by looking at

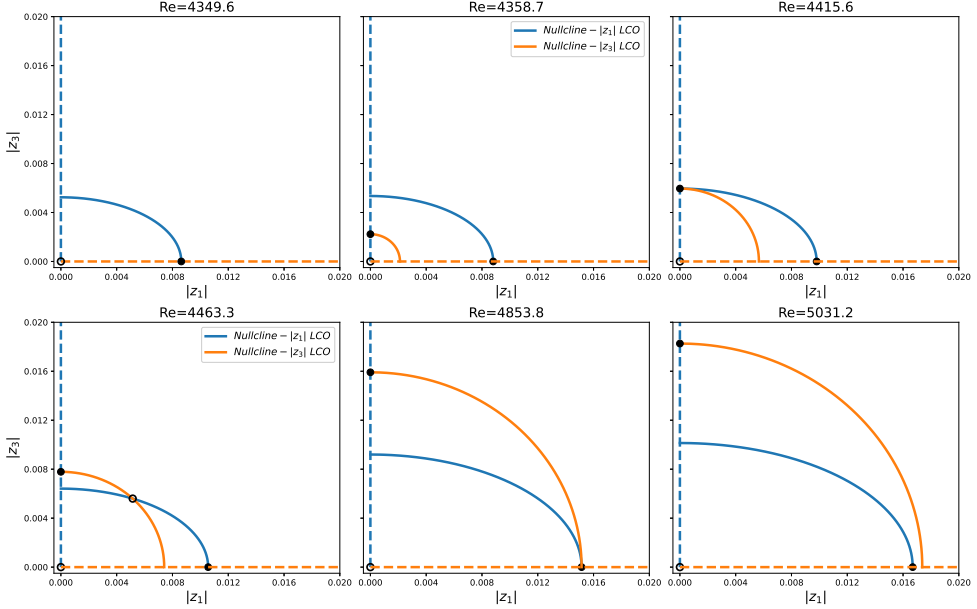


Figure 3: Evolution of the LCO null-clines as the Reynolds number is increased past the first bifurcation point. The solid blue line indicates the null-cline of the $\lambda_{1,2}$ LCO emerging from the first bifurcation. The solid orange line indicates the null-clines of the $\lambda_{3,4}$ LCO emerging from the second bifurcation point. The intersection of these LCO null-clines produces the quasi-periodic edge-state.

287 the Reynolds number dependent multiplier of $|z_3|^2$ in equation (3.2b), given by,

$$288 \quad d|z_3|^2/dt = \alpha_3(\epsilon)|z_3|^2$$

$$289 \quad \alpha_3(\epsilon) = 3.603\epsilon + 2.0\sigma' + 1.262\epsilon^2 - 0.011\epsilon\sigma' - 1658.8|z_1(\epsilon)|^2,$$

290 where, $|z_1(\epsilon)|$, is the Reynolds number dependent equilibrium value of $|z_1|$ for
291 $|z_3| = 0$. When $\alpha_3(\epsilon)$ first becomes non-negative, is the new “path dependent”
292 bifurcation point. This is found to coincide with $\tilde{Re}_4 = 4853.8$. At this point, the
293 $\lambda_{1,2}$ LCO becomes unstable, since, any increase in z_3 strengthens the saturation
294 mechanism provided by the cross interaction terms for $\lambda_{1,2}$ LCO, and therefore
295 reduces the equilibrium value of $|z_1|$. This reduction in $|z_1|$ implies the effective
296 growth rate for z_3 becomes larger, and a feedback loop is established, moving the
297 system away from the fixed point on the $|z_1|$ axis, ending up at fixed point on
298 the $|z_3|$ axis, and the system now exhibits the $\lambda_{3,4}$ LCO. The system now follows
299 this new fixed point with further slow increases in Reynolds numbers.

300 The phenomenon repeats itself with the roles of the two limit cycles switched
301 when the system is slowly varied in the opposite direction. For a high enough
302 Reynolds number the $\lambda_{3,4}$ LCO exists and the system is at the equilibrium
303 point on $|z_3|$ axis. Again, the non-zero $|z_3|$ causes z_1 to have a damped effective
304 eigenvalue, thereby suppressing the emergence of the $\lambda_{1,2}$ LCO. The effective
305 growth rate along the decreasing Reynolds number path is again predicted using
306 the terms linear in $|z_1|^2$ in equation (3.2a),

$$307 \quad \alpha_1(\epsilon) = 1.669\epsilon + 0.649\epsilon^2 - 0.007\epsilon\sigma' - 3107.6|z_3(\epsilon)|^2,$$

308 where $|z_3(\epsilon)|$ is the Reynolds number dependent equilibrium value of $|z_3|$. As one

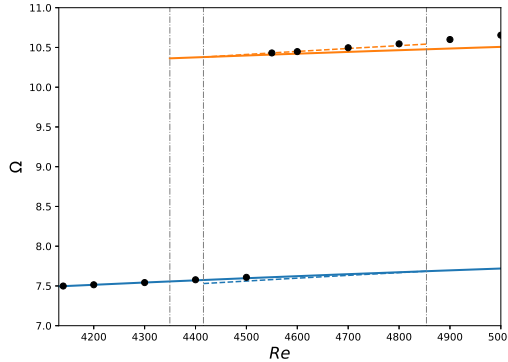


Figure 4: Comparison of the angular frequencies of the full system and the reduced model. The blue line indicates the $\lambda_{1,2}$ LCO angular frequencies while the orange line indicates the $\lambda_{3,4}$ LCO angular frequencies. The solid black circles indicate the frequencies obtained from non-linear simulations.

309 might anticipate, $\alpha_1(\epsilon)$ becomes non-negative at \widetilde{Re}_3 and the same feedback loop
 310 described earlier, now causes the system to move away from the $\lambda_{3,4}$ LCO and
 311 reach the $\lambda_{1,2}$ LCO equilibrium point. The $\lambda_{1,2}$ LCO remains stable below \widetilde{Re}_3
 312 until the first bifurcation point is reached. Between \widetilde{Re}_3 and \widetilde{Re}_4 the system
 313 would exhibit bistability.

314 Finally, since the amplitudes at the equilibrium points are known through the
 315 reduced equations, the equilibrium frequencies can also be predicted. This is
 316 shown in figure 4. The blue line indicates the angular frequencies for the $\lambda_{1,2}$
 317 LCO equilibrium point, while the orange line indicates the angular frequencies for
 318 the $\lambda_{3,4}$ LCO. The dashed lines indicate the angular frequencies for the respective
 319 modes at the quasi-periodic edge state. The filled black circles indicate the results
 320 obtained through the non-linear simulations. The $\lambda_{1,2}$ LCO angular frequencies
 321 are well predicted while a small deviation exists for the $\lambda_{3,4}$ LCO at higher
 322 Reynolds numbers. This would be typical of an asymptotic reduction where, the
 323 errors increase as the system is moved further away from the (first) bifurcation
 324 point.

325 4. Conclusion

326 A reduced mathematical model for the flow in an open cavity is presented. The
 327 model is derived through a center manifold manifold reduction of a perturbed
 328 system resulting in a co-dimension two bifurcation point. The original system is
 329 then approximated asymptotically, along with the Reynolds number and center
 330 subspace mode variations, resulting in a normal form of a Reynolds number
 331 dependent double Hopf bifurcation. The model exhibits many of the key char-
 332 acteristics of the system found in the detailed study by Bengana et al. (2019),
 333 including existence of bistability, switching of the stability of the limit cycles
 334 and a quasi-periodic edge state between the two limit cycles. The reduced model
 335 provides a mechanism for the switching of the stability of the two limit-cycle
 336 oscillations based on the cross-interaction term and effective eigenvalue of the
 337 modes at the equilibrium points of the limit-cycles, and also predicts the Reynolds
 338 number values where the switching of stability occurs.

REFERENCES

- 339 Barbagallo, A., Sipp, D., and Schmid, P. J. (2009). Closed-loop control of an open cavity flow
 340 using reduced-order models. *Journal of Fluid Mechanics*, 641:1–50.
- 341 Bengana, Y., Loiseau, J.-C., Robinet, J.-C., and Tuckerman, L. S. (2019). Bifurcation analysis
 342 and frequency prediction in shear-driven cavity flow. *Journal of Fluid Mechanics*,
 343 875:725–757.
- 344 Carini, M., Auteri, F., and Giannetti, F. (2015). Centre-manifold reduction of bifurcating flows.
 345 *Journal of Fluid Mechanics*, 767:109–145.
- 346 Carr, J. (1982). *Applications of centre manifold theory*, volume 35. Springer Science & Business
 347 Media.
- 348 Carr, J. and Muncaster, R. G. (1983). The application of centre manifolds to amplitude
 349 expansions. i. ordinary differential equations. *Journal of Differential Equations*,
 350 50(2):260–279.
- 351 Coullet, P. H. and Spiegel, E. A. (1983). Amplitude equations for systems with competing
 352 instabilities. *SIAM Journal on Applied Mathematics*, 43(4):776–821.
- 353 Cox, S. M. and Roberts, A. J. (1991). Centre manifolds of forced dynamical systems. *The Journal
 354 of the Australian Mathematical Society. Series B. Applied Mathematics*, 32(4):401–436.
- 355 Fischer, P. F., Lottes, J. W., and Kerkemeier, S. G. (2008). Nek5000 web page. <http://nek5000.mcs.anl.gov>.
- 356 Guckenheimer, J. and Holmes, P. (1983). *Nonlinear Oscillations, Dynamical Systems, and
 358 Bifurcations of Vector Fields*. Springer Science & Business Media New York.
- 359 Hochs, P. and Roberts, A. (2019). Normal forms and invariant manifolds for nonlinear, non-
 360 autonomous pdes, viewed as odes in infinite dimensions. *Journal of Differential Equations*,
 361 267(12):7263–7312.
- 362 Jain, S. and Haller, G. (2022). How to compute invariant manifolds and their reduced dynamics
 363 in high-dimensional finite element models. *Nonlinear dynamics*, 107(2):1417–1450.
- 364 Loiseau, J.-C. and Brunton, S. L. (2018). Constrained sparse galerkin regression. *Journal of
 365 Fluid Mechanics*, 838:42–67.
- 366 Mantić-Lugo, V., Arratia, C., and Gallaire, F. (2015). A self-consistent model for the saturation
 367 dynamics of the vortex shedding around the mean flow in the unstable cylinder wake.
 368 *Physics of Fluids*, 27(7).
- 369 Meliga, P. (2017). Harmonics generation and the mechanics of saturation in flow over an open
 370 cavity: a second-order self-consistent description. *Journal of Fluid Mechanics*, 826:503–
 371 521.
- 372 Mercer, G. N. and Roberts, A. J. (1990). A centre manifold description of contaminant dispersion
 373 in channels with varying flow properties. *SIAM Journal on Applied Mathematics*,
 374 50(6):1547–1565.
- 375 Negi, P. S. (2024). Asymptotic center-manifold for the navier–stokes. *arXiv preprint
 376 arXiv:2411.03727*.
- 377 Negi, P. S. (2026). Constructing asymptotic center manifold for extended systems. *submitted to
 378 Nonlinear Dynamics*.
- 379 Patera, A. T. (1984). A spectral element method for fluid dynamics: Laminar flow in a channel
 380 expansion. *Journal of Computational Physics*, 54(3):468 – 488.
- 381 Roberts, A. J. (2014). *Model emergent dynamics in complex systems*. SIAM.
- 382 Roberts, A. J. (2022). Backwards theory supports modelling via invariant manifolds for non-
 383 autonomous dynamical systems.
- 384 Rowley, C. W. and Williams, D. R. (2006). Dynamics and control of high-reynolds-number flow
 385 over open cavities. *Annu. Rev. Fluid Mech.*, 38(1):251–276.
- 386 Sipp, D. and Lebedev, A. (2007). Global stability of base and mean flows: a general approach
 387 and its applications to cylinder and open cavity flows. *Journal of Fluid Mechanics*,
 388 593:333–358.
- 389 Sipp, D., Marquet, O., Meliga, P., and Barbagallo, A. (2010). Dynamics and control of
 390 global instabilities in open-flows: A linearized approach. *Applied Mechanics Reviews*,
 391 63(3):030801.
- 392 Stewart, G. W. (2002). A Krylov–Schur algorithm for large eigenproblems. *SIAM Journal on
 393 Matrix Analysis and Applications*, 23(3):601–614.
- 394 Vizzaccaro, A., Gobat, G., Frangi, A., and Touzé, C. (2024). Direct parametrisation of invariant

- 395 manifolds for non-autonomous forced systems including superharmonic resonances.
396 *Nonlinear Dynamics*, 112(8):6255–6290.
- 397 Wiggins, S. (2003). *Introduction to Applied Nonlinear Dynamical Systems and Chaos*. Springer-
398 Verlag New York.